Lawrence Berkeley National Laboratory
Recent Work

Title
Multipoles induced by inter-strand coupling currents in LARP Nb3Sn quadrupoles

Permalink
https://escholarship.org/uc/item/2xn4912z

Journal
IEEE Transactions on Applied Superconductivity, 24(3)

ISSN
1051-8223

Authors
Wang, X
Ambrosio, G
Borgnolutti, F
et al.

Publication Date
2014

DOI
10.1109/TASC.2013.2285235

Peer reviewed

eScholarship.org Powered by the California Digital Library
University of California

Multipoles Induced by Inter-Strand Coupling Currents in LARP Nb_3Sn Quadrupoles

X. Wang, G. Ambrosio, F. Borgnolutti, M. Buehler, G. Chlachidze, D. R. Dietderich, J. DiMarco, H. Felice, P. Ferracin, A. Ghosh, A. Godeke, M. Marchevsky, D. Orris, S. O. Prestemon, G. Sabbi, C. Sylvester, M. Tartaglia, E. Todesco, G. Velev, and P. Wanderer

***Abstract*—The U.S. LHC Accelerator Research Program has been developing Nb_3Sn quadrupole magnets of progressively increasing performance and complexity for the High-Luminosity LHC project. The magnets are wound with Rutherford cables following the wind-and-react process. The resulting inter-strand coupling can generate strong field distortions during current ramp. The latest series of 120 mm aperture magnets (HQ) are designed and built for high field quality, offering an opportunity for detailed studies of these effects. Magnetic measurements of first-generation HQ magnets showed strong ramp-rate dependence. A stainless-steel core was introduced for the second generation of magnet coils to control the inter-strand coupling currents and the resulting dynamic multipoles. We report the observed dynamic effects and compare with calculations taking into account the coil geometry and cross-contact resistance in the Rutherford cable. In particular, the dependence of field quality on width and position of the stainless steel core is discussed.**

***Index Terms*—Field quality, inter-strand coupling currents, Nb_3Sn accelerator magnets, Rutherford cable.**

I. Introduction

RUTHERFORD cables are extensively used to wind superconducting accelerator magnets where high current and low inductance are desirable [1]. During the field ramp, coupling currents are induced between the filaments inside the strands and between the strands in the cable. This leads to energy loss and field distortions, both systematic and random, that may deteriorate the accelerator performance [2], [3].

In Nb_3Sn Rutherford cables, the inter-strand coupling currents (ISCC) dominate over the inter-filament coupling currents since the Cu layer of the strands sinter during the heat treatment. Field errors induced by ISCC were observed in previous Nb_3Sn accelerator model magnets [4]–[6]. In analysis of these effects, the cross (R_c) and adjacent (R_a) contact resistance are identified to characterize the ISCC in the framework of network model [7]. A resistive core in the cable can be used to suppress the ramp-rate effect in Nb_3Sn cables and magnets [8]–[10]; this is compatible with the heat treatment and allows for preservation of a low R_a for current sharing and stability purposes.

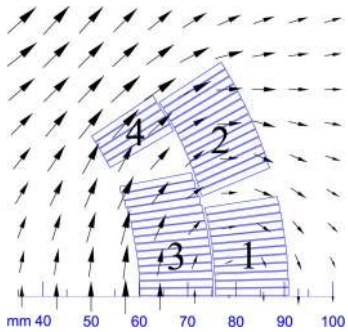

Fig. 1. Field vectors in HQ magnet at 10 kA with one octant of coil shown. Coil blocks 1 and 2 are in the outer layer; 3 and 4 are in the inner layer.

Strong field distortions during current ramp were observed in HQ01, the first-generation Nb_3Sn quadrupole magnets with accelerator features developed by the U.S. LHC Accelerator Research Program (LARP) [11], [12] for the High-Luminosity LHC (HL-LHC) project [13], [14]. The effect was correlated to the low R_c in the Rutherford cable and a stainless steel core was introduced for the second generation of coils to suppress the effect based on the extensive study of various core configurations [15]. Here we report the measured ramp-rate effects in both HQ01 and HQ02, giving an estimate of the R_c, and analyze the impact of core configuration on the ISCC multipoles. The magnetic measurements of HQ02a and general overview of its field quality were reported in [16].

II. HQ Magnets and Cables

The 120 mm aperture HQ magnet consists of four double-layer $\cos 2\theta$ coils and is designed with accelerator features such as alignment and field quality [17]–[19]. The four coil blocks present in an octant are shown in Fig. 1.

Keystoned Rutherford cables were made at the LBNL cabling facility [20]. Major parameters of the cables used in HQ01e and HQ02a are compared in Table I. A stainless steel

Manuscript received August 1, 2013; accepted October 2, 2013. Date of publication October 9, 2013; date of current version November 8, 2013. This work was supported by the U.S. LHC Accelerator Research Program through U.S. Department of Energy contracts DE-AC02-07CH11359, DE-AC02-98CH10886, DE-AC02-05CH11231, and DE-AC02-76SF00515. The HiLumi LHC Design Study is included in the High Luminosity LHC project and is partly funded by the European Commission within the Framework Programme 7 Capacities Specific Programme, Grant Agreement 284404.

X. Wang, F. Borgnolutti, D. R. Dietderich, H. Felice, A. Godeke, M. Marchevsky, S. O. Prestemon, and G. Sabbi are with Lawrence Berkeley National Laboratory (LBNL), Berkeley, CA 94720 USA (e-mail: xrwang@lbl.gov).

G. Ambrosio, M. Buehler, G. Chlachidze, J. DiMarco, D. Orris, C. Sylvester, M. Tartaglia, and G. Velev are with Fermi National Accelerator Laboratory (FNAL), Batavia, IL 80510 USA.

P. Ferracin and E. Todesco are with European Organization for Nuclear Research (CERN), CH-1211 Geneva, Switzerland.

A. Ghosh and P. Wanderer are with Brookhaven National Laboratory (BNL), Upton, NY 11973 USA.

Color versions of one or more of the figures in this paper are available online at http://ieeexplore.ieee.org.

Digital Object Identifier 10.1109/TASC.2013.2285235

1051-8223 © 2013 IEEE

TABLE I
RUTHERFORD CABLES FOR HQ01e AND HQ02a

Parameter	Unit	HQ01e	HQ02a
Strand number	-	35	
Core material	-	-	SS316L
Nominal strand diameter	mm	0.80	0.778
Cable pitch length	mm	102	95
Bare cable width	mm	15.15	14.77
Bare cable mid thickness	mm	1.437	1.376
Keystone angle	deg.	0.75	0.73
Twist pitch	mm	14±2	

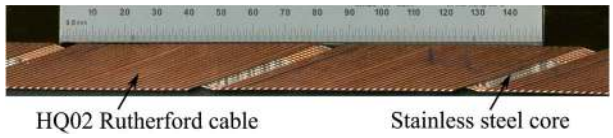

Fig. 2. Cored Rutherford cable for the HQ magnet. The core is 8 mm wide and biased towards the cable thick edge. Photo courtesy of H. Higley of LBNL.

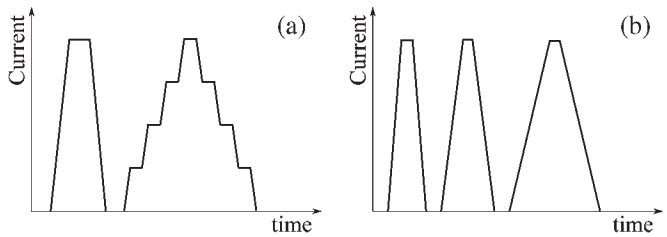

Fig. 3. Current profiles for (a) stair-step and (b) loop measurements.

316L core was used in HQ02a for the first time in LARP Nb_3Sn model magnets. The selected core configuration is 8 mm wide and 25 μm thick, with bias towards the cable thick edge (Fig. 2), yielding about 60% coverage within the available space between the two rows of strands.

III. MEASUREMENT PROTOCOL AND DATA REDUCTION

The nominal ramp rate for HQ magnets is 13 A/s. Two types of measurements were used to obtain the dynamic components, using ramp rates in the range 10–100 A/s. First, the static multipoles at various current levels were measured with a stair-step measurement along the load line [Fig. 3(a)]. Then, a loop measurement was performed with various ramp rates and no cleansing quench in between [Fig. 3(b)]. Both measurements were preceded by a pre-cycle to set the magnet into a reproducible state.

The magnetic field in the aperture of the straight section of a quadrupole can be expressed as

$$B_y + i\,B_x = \sum_{n=1}^{\infty} C_n \left(\frac{x + i\,y}{R_{\rm ref}}\right)^{n-1}, \qquad (1)$$

where $C_n = B_n + iA_n$ is the complex multipole coefficient in T at the reference radius $R_{\rm ref}$ [21]. B_n and A_n are the normal and skew multipole coefficients, respectively. $R_{\rm ref}$ is 40 mm for HQ magnet. For a certain ramp rate r and current I, the dynamic multipole component can be obtained by subtracting the static component given by the stair-step measurements from the total multipole given by the loop measurements, i.e., $C_n^{\rm dynamic}(r, I) = C_n^{\rm loop}(r, I) - C_n^{\rm stairstep}(I)$. The normalized harmonics is given by

$$c_n^{\rm dynamic}(r, I) = \frac{C_n^{\rm dynamic}(r, I)}{B_2^{\rm stairstep}(I)} \times 10^4, \qquad (2)$$

where $c_n = b_n + i\,a_n$ is expressed in unit. Details regarding the rotating probes, measurement system and data reduction can be found in [16], [22], [23].

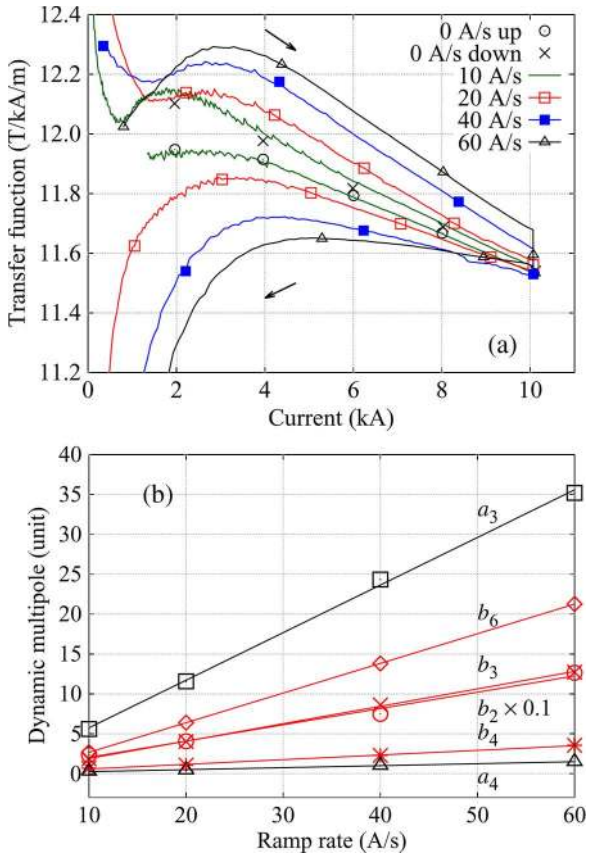

Fig. 4. HQ01e ramp-rate dependence of (a) main field transfer function and (b) normalized low-order dynamic multipoles at 10 kA, 4.5 K. The ramp direction is marked by the arrows in (a). 0 A/s data are from the stair-step measurements. Solid lines in (b) are the least-square linear fit of the measured dynamic multipoles. $R_{\rm ref} = 40$ mm.

IV. HQ01e MAGNET WITH NONCORED CABLE

A. Field Distortion During Current Ramp

After several cycles of HQ01 assembly and test aimed at establishing the required performance baseline [24]–[26], a comprehensive set of magnetic measurements was performed in the HQ01e model. Pronounced ramp-rate dependence of the field quality was observed [Fig. 4(a)], accompanied by strong ramp-rate sensitivity of the quench performance [25], [26]. The phenomenon is relevant even at 10 A/s which is lower than the nominal ramp rate. The different trends seen in Fig. 4(a) between the up- and down-ramps are due to the magnetization effect from ISCC and persistent current. Fig. 4(b) gives an example of the dynamic multipoles in units, as determined by (2).

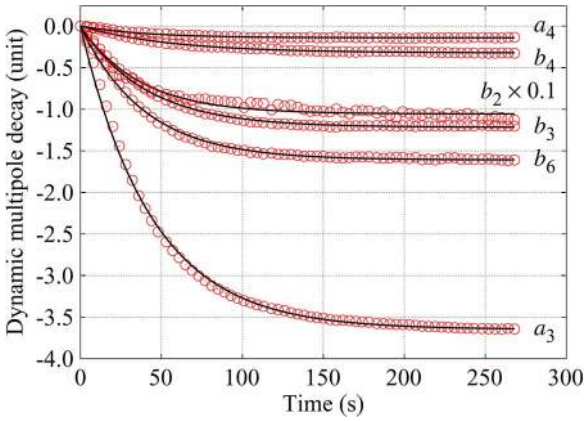

Fig. 5. Exponential decay of the normalized main field and low-order multipoles of HQ01e at 14 kA, 4.5 K (81% short-sample limit, SSL). The ramp rate reduced from 10 A/s to 0 at time 0. The data traces were translated to a common reference at time 0, to enable a direct comparison of the dynamic decay. Open circles: measurement. Solid lines: exponential fit. $R_{\mathrm{ref}} = 40$ mm.

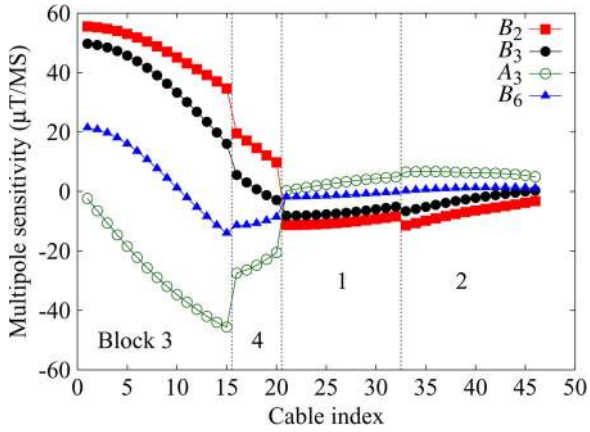

Fig. 6. G_{c} sensitivity of multipoles of each individual turn in one octant of the coil (Fig. 1) at 10 kA with a ramp rate of 13 A/s. $R_{\mathrm{ref}} = 40$ mm.

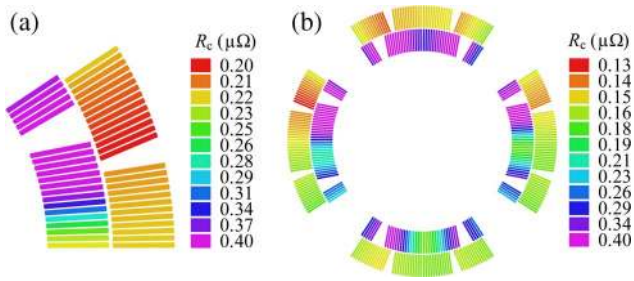

Fig. 7. Possible R_{c} profiles for HQ01e to match (a) the measured ISCC B_2 and B_6 and (b) the measured ISCC multipoles up to $n = 6$.

Main field and low-order multipole decays were observed at each current level of the stair-step measurements (Fig. 5). The decay can be described with a single time constant for a resistive process according to $c_n(t) = c_n^{\infty}[1 - \exp(-t/\tau)]$, where the decay amplitude c_n^{∞} is identical to the normalized dynamic multipole as given in (2), neglecting the measurement uncertainty. The time constant τ for the main field and low-order multipoles is between 40 and 50 s at current levels between 8 and 14 kA.

The observed linear ramp-rate dependence of the dynamic multipole amplitude and its exponential decay with a large time constant suggest that the ISCC is the primary source for the observed field distortion. The time constant for the inter-filament coupling current was estimated to be of the order of 1–10 ms for HQ strand, at least three orders of magnitude lower than the observed decay time constant. Neither could it stem from the boundary-induced coupling currents because of comparable results obtained using probes of different lengths [23].

B. Analysis of the Cross-Contact Resistance in HQ01e

The amplitude of the field generated by the ISCC can be given by $B_{\mathrm{ISCC}} = \alpha \dot{B}_{\perp} G_{\mathrm{c}}$, where α is a constant determined by the cable geometry, $\dot{B}_{\perp}$ is the sweep rate of the field perpendicular to the cable broad surface, and $G_{\mathrm{c}}(= 1/R_{\mathrm{c}})$ is the cross-contact conductance with contribution of R_{a} neglected here [7]. Fig. 6 shows the sensitivity in each individual turn at 10 kA, 13 A/s determined by a computation based on the network model [7], [27]. The inner layer turns, in particular those located near the mid-plane, see a higher $B_{\perp}$ and hence have higher sensitivity.

The G_{c} profile across the magnet cross section and the measured field error can be related as

$$\mathbf{B}_{\mathrm{ISCC}} = \mathbf{S}\mathbf{G}_{\mathrm{c}}^{\mathrm{T}}, \tag{3}$$

where $\mathbf{B}_{\mathrm{ISCC}}$ is the field error vector of length n, $\mathbf{G}_{\mathrm{c}}$ is the cross-contact conductance vector of length m, and $\mathbf{S}$ the sensitivity matrix of size $n \times m$. The conductance profile can then be determined given the $\mathbf{B}_{\mathrm{ISCC}}$ and $\mathbf{S}$. A similar approach was used to determine the coil block displacement based on the geometric harmonics [28], [29]. A direct solution of (3) is possible when $m \leq n$. This yields $R_{\mathrm{c}} = 0.40$ $\mu\Omega$ for the entire cross section to match the measured ISCC B_2, and $R_{\mathrm{c}} = 0.14$ $\mu\Omega$ to reproduce the measured ISCC B_6. No single physical R_{c} exists if ISCC B_2 and B_6 are to be matched simultaneously, indicating that R_{c} is not uniform across the magnet cross section. Nevertheless, this range is consistent with a $R_{\mathrm{c}} = 0.33$ $\mu\Omega$ measured on a prototype HQ cable without core [30].

When the number of unknown G_{c} is larger than the number of known field errors $(m > n)$, multiple solutions exist for (3). In this case, we follow the approach proposed in [31], [32] to obtain a possible R_{c} profile that reproduces the measured field errors under certain assumptions. The R_{c} profile calculated for a range between 0.20 and 0.40 $\mu\Omega$ is shown in Fig. 7(a). The discrepancy between the measured and calculated ISCC B_2 and B_6 at 10 kA, 40 A/s is less than 3%. The outer layer has a more uniform R_{c} distribution (the standard deviation σ is 6.6 nΩ, 3% of the outer layer mean value) compared to the inner layer ($\sigma = 66$ nΩ, 19% of the inner layer mean value). The sensitivity of the decay time constant is 12.3 s/MS which gives 30–61 s based on the estimated R_{c} range, consistent with the measurement. Nevertheless, it should be stressed that a range of possible solutions exist depending on the assumption used for optimization, and therefore the profiles in Fig. 7 have only qualitative value.

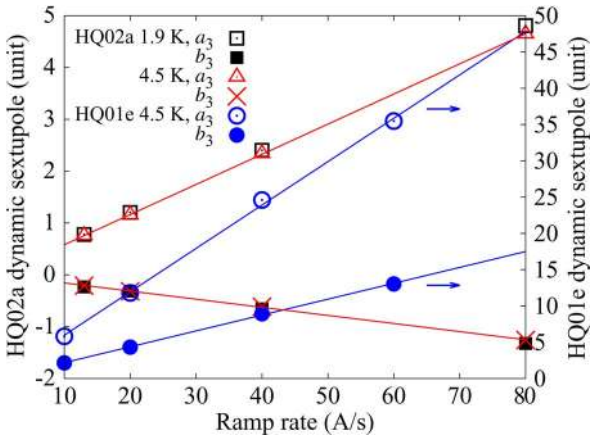

Fig. 8. Comparison of dynamic sextupoles as a function of ramp rate between HQ02a (primary y-axis) and HQ01e (secondary y-axis) at 10 kA. The solid lines are least-square linear fits of the data. $R_{\rm ref} = 40$ mm.

Using a similar approach, a possible $R_{\rm c}$ profile that matches the measured ISCC multipoles of both allowed and nonallowed orders is shown in Fig. 7(b). This profile reproduces the measured harmonics with less than 5% discrepancy. A top-bottom $R_{\rm c}$ asymmetry appears for a nominal coil cross section, consistent with the strong ramp-rate sensitivity of a_3 [Fig. 4(b)]. For HQ01e, the Rutherford cables for the top two coils had a stronger oxidization than the cables for the bottom two coils after annealing. The oxide layer may enhance $R_{\rm c}$ in a way consistent with the observed effect; however it is not clear if the effect of oxidization is preserved during the coil curing and heat treatment following the magnet winding. With this profile, the $R_{\rm c}$ in the inner layer again varies more than that of the outer layer. In the inner layer, the σ of the coil block $R_{\rm c}$ is 58 nΩ, 19% of the $R_{\rm c}$ averaged from all inner layer coil blocks; in the outer layer, $\sigma = 8$ nΩ, 5% of the $R_{\rm c}$ averaged from all outer layer coil blocks. The difference between the layer $R_{\rm c}$, consistent with the computed sensitivity (Fig. 6), was also observed in SSC and LHC NbTi magnets [31], [32]. It implies that the difference of $R_{\rm c}$ between the cables and coils should be minimized particularly in the inner layer to limit the ISCC multipoles. We will attempt to quantify the impact of random $R_{\rm c}$ in Section VI.

V. HQ02a With Cored Cable

HQ02a showed a significantly reduced ramp-rate sensitivity in the main field and other low-order harmonics compared to HQ01e [16]. In addition, no quench was observed up to 15 kA (80% SSL) for ramp rates up to 200 A/s at 1.9 K [33]. Fig. 8 compares the amplitudes of the measured dynamic sextupoles of HQ01e and HQ02a at 10 kA. For the same ramp rate, the amplitude of the dynamic sextupoles in HQ02a is 10–13 times lower than in HQ01e. The ramp-rate sensitivity of a_3 and b_3 for HQ02a at 10 kA, 1.9 K are 0.06 and -0.017 unit/(A/s), respectively. The difference in the ramp-rate sensitivity between 1.9 K and 4.5 K for HQ02a is less than 8%, indicating no significant temperature dependence of ISCC between 1.9 K and 4.5 K.

TABLE II
Comparison of the Dynamic Harmonics at 13 A/s, 14 kA (Unit at $R_{\rm ref} = 40$ mm). η Is the Compensation Factor

Harmonics	HQ01e	HQ02a	η
b_2	14.60	0.85	0.94
b_3	1.56	-0.12	1.08
b_4	0.43	0.04	0.90
b_5	0.21	-0.00	1.02
b_6	2.09	0.10	0.95
a_3	4.73	0.44	0.91
a_4	0.18	-0.14	1.75
a_5	0.52	0.12	0.77
a_6	-0.26	-0.04	0.84

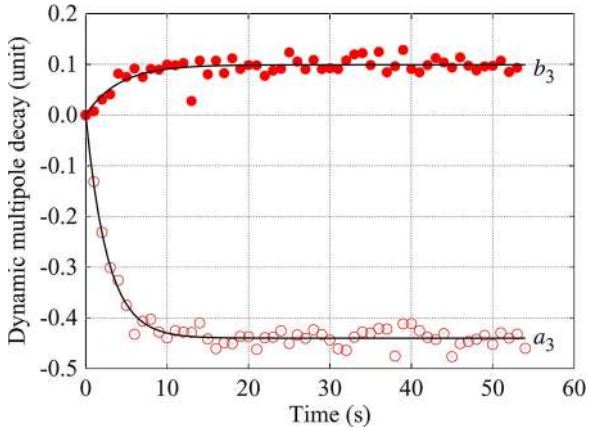

Fig. 9. Exponential decay of the normalized HQ02a sextupoles at 14 kA, 1.9 K (77% SSL). The ramp rate reduced from 13 A/s to 0 at time 0. The data traces were translated to a common reference at time 0, to enable a direct comparison of the dynamic decay. Symbols: measurement. Solid lines: exponential fit. $R_{\rm ref} = 40$ mm.

The normalized dynamic multipoles at 13 A/s, 14 kA are compared between HQ01e and HQ02a in Table II. The HQ01e harmonics are scaled from the measurements performed at 10 A/s and the HQ02a data are directly from the 13 A/s measurements. Positive dynamic harmonics add to the static field [34] whereas the negative ones cancel the static field. The compensation factor based on the dynamic harmonics between two magnets, $\eta_n = 1 - c_n({\rm HQ02a})/c_n({\rm HQ01e})$, is also shown. When $\eta_n = 1$, the dynamic multipole of order n is completely removed whereas $\eta > 1$ and $\eta < 1$ correspond to the over and under compensation, respectively. It is preferred to have $\eta \approx 1$ because the dynamic harmonics and field distortions are present during current ramp with strong over or under compensation.

The cored cable in HQ02a effectively reduced the ISCC multipole as η is within 1 ± 0.23 except a_4 where a significant over compensation occurred. The contribution from the 10% difference in the cable constant α (Section IV-B) due to the wider cable and longer pitch in HQ01e is negligible (less than 0.02 change in η except that for a_4, η increases from 1.75 to 1.83).

The HQ02a stair-step measurements showed exponential decay in low-order multipoles, in particular the sextupoles (Fig. 9). The time constant ranged from 2 to 5 s, a factor $\sim$10 smaller than HQ01e. Decay in b_2 and b_6, however, are not obvious in the stair-step measurements.

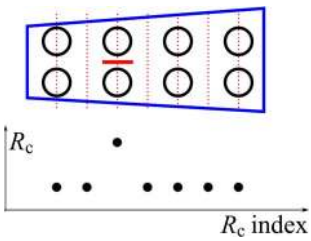

Fig. 10. A unit core (red solid line) covering a single cross contact (red dashed line). The core is represented by a R_c value higher than those of the noncored area.

For a direct comparison to HQ01e, a uniform R_c profile along the cable width is first assumed for HQ02a as an equivalent R_c. The direct calculation gives an equivalent R_c ranging from 2.2 to 3.9 $\mu\Omega$ based on the measured ISCC B_2 and B_6. This is about an order of magnitude increase compared to the R_c value in HQ01e. The computed time constant ranges from 3–6 s, consistent with the measurement. The measured ISCC multipoles can be reproduced within 2% based on the indirect method for an equivalent R_c ranging from 2 to 7 $\mu\Omega$ assuming a nominal coil cross section. In the inner layer, the σ of the coil block R_c is 1.2 $\mu\Omega$, 28% of the R_c averaged from all inner layer coil blocks; in the outer layer, $\sigma = 0.2$ $\mu\Omega$, 5% of the R_c averaged from all outer layer coil blocks.

While the above considerations can provide a useful estimate of the average R_c, a strong variation is expected within each turn due to the partial core coverage in HQ02a, leading to a nonuniform R_c profile along the cable width. To estimate the ISCC multipoles from a detailed R_c profile, a computational code based on the network model [35] was applied and further developed for this application (program EDDY). A cored cable is treated as a R_c profile along the cable width characterized by the core coverage and different R_c values in the cored and noncored area. Fig. 10 shows a profile of a unit core covering a single strand crossing.

Based on the nominal core location in HQ02a and assuming $R_c = 50$ $\mu\Omega$ at the cored area [36] and $R_c = 0.2$ $\mu\Omega$ in the outer layer noncored area, one obtains reasonable agreement (within 12%) between the measured and calculated ISCC b_2 and b_6 with the $R_c = 0.75$ $\mu\Omega$ in the inner layer noncored area as the free parameter.

VI. Impact of Core Configuration

In a cored cable, the R_c is affected by the core configuration, e.g., its width and position within the cable. Here we attempt to obtain some insight on the impact of core configuration on the ISCC multipoles and their reproducibility. Since the contribution of R_a is typically less than 15% of ISCC multipole, it is neglected in the following analysis.

A sweep of a unit core (Fig. 10) moving from the inner layer to outer layer was performed based on the nominal HQ cross section (Fig. 1). The ISCC B_2 is suppressed when the unit core is in the inner layer while it is enhanced when the core moves to the outer layer (Fig. 11). This can be explained qualitatively by the opposite directions of the $B_\perp$ in two layers and hence the polarity of the induced ISCC (Figs. 1 and 6). The effect peaks

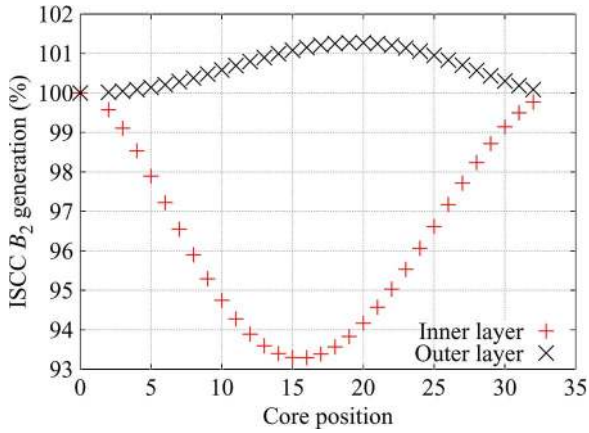

Fig. 11. Comparison of the ISCC B_2 generation from a unit core as a function of its position in different layers of HQ. The generation is normalized to the no-core case plotted at core position 0. Other core positions correspond to the R_c index in Fig. 10. Assuming $R_c = 50$ $\mu\Omega$ for the cored area and 0.5 $\mu\Omega$ for the noncored area. $R_{ref} = 40$ mm.

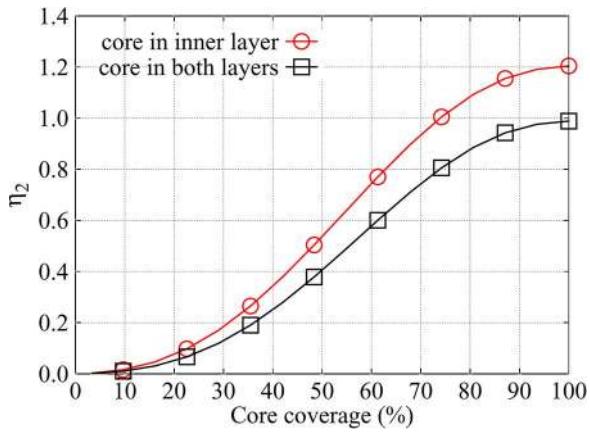

Fig. 12. The compensation factor η for ISCC B_2 with increasing core coverage from the cable thick edge in HQ. η is defined in Section V. $R_c = 50$ $\mu\Omega$ for the cored area and 0.5 $\mu\Omega$ for the noncored area. $R_{ref} = 40$ mm.

when the core is located near the center of the cable which minimizes the area of the eddy-current loops. Similar behavior was observed for ISCC B_6.

Following the linearity of multipole field and Biot-Savart law, the ISCC multipoles due to a given R_c profile can be obtained by combining each individual R_c in the profile. Thus, based on Fig. 11, the suppression of ISCC with an arbitrary core configuration can be studied. Here we compare two cases, A) core is implemented in both layers and B) core is implemented in inner layer only. For both cases, the core starts from the cable thick edge which is the preferred approach to make the cable more mechanically stable and less prone to degradation due to strand compaction at the thin edge. Fig. 12 compares the compensation factor of each case for the HQ magnet.

Both cases can completely remove ISCC B_2 ($\eta_2 = 1$): a 100% core coverage is necessary for case A whereas 74% of coverage is sufficient for case B. An over compensation with the static B_2 being canceled by the dynamic B_2 would occur if the core covered more than 74% for case B.

The effect of random R_c variations was studied by assuming R_c is uniform in each coil block but varies among coil blocks.

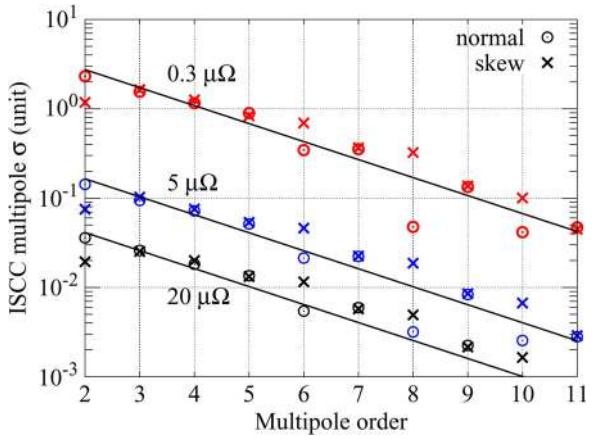

Fig. 13. Random ISCC field error (1σ) of HQ as a function of harmonic order with various mean R_c values and 20% variation of R_c among coil blocks at 15 kA, 13 A/s ramp rate. Solid lines are the power low fit. $R_{ref} = 40$ mm.

A normal distribution with mean target R_c values and 20% of the mean value as the σ is used and 500 cases were computed. The standard deviation of the resulting ISCC multipoles can be described by a power law as $\sigma(a_n, b_n) = G_c \alpha \beta^n$, where a_n and b_n is the ISCC harmonics normalized to the static main field and α, β the fitting parameters. A similar power law is used to describe the effect of random coil block displacement [37]. At 15 kA (the nominal operation level for HQ magnet), we have $\alpha = 2.08$ $\mu\Omega$ and $\beta = 0.63$ with the mean R_c ranging from 0.1 $\mu\Omega$ to 100 $\mu\Omega$ (Fig. 13). One would need a mean R_c of at least 8 $\mu\Omega$ to limit the random error of ISCC multipoles at the nominal level below 0.1 units, assuming 20% of variation of R_c among coil blocks. For the same variation, lower mean R_c leads to higher random error emphasizing the advantage of a high R_c. A more uniform R_c is necessary to reach the same random error level with a lower mean R_c. For example, 10% variation is required with a mean R_c of 3.3 $\mu\Omega$ for the same 0.1 units threshold.

A case with 20% variation in the inner layer R_c and 5% variation in the outer layer R_c, consistent with the results in Section IV-B, was also considered. Since the dynamic multipoles are less sensitive to the outer layer R_c, the resulting α is within 5% of the case with identical R_c variation in both layers ($\alpha = 1.98$ and $\beta = 0.63$). This again indicates the significance of uniform R_c in the inner layer.

VII. Conclusion

Ramp-rate dependence of the field quality was studied on the LARP HQ01 and 02 magnets in support of the design of the interaction region quadrupoles for HL-LHC. Strong ramp-rate dependence of the field errors was observed in HQ01 and was correlated to the low cross-contact resistance (0.2–0.4 $\mu\Omega$) in the Rutherford cables. To suppress these field distortions during current ramp, a stainless steel core was introduced in HQ02a with 60% coverage, biased toward the cable thick edge. Significant reduction of the inter-strand coupling currents (ISCC) was experimentally confirmed. Compared to HQ01e, the ISCC induced field error in the main field decreased from 14.60 to 0.85 units at 14 kA with 13 A/s ramp rate whereas low-order harmonics up to order of 6 were less than 0.44 units, 10 times smaller than those of HQ01e. The analysis suggests that the equivalent R_c in HQ02a ranged from 2 to 7 $\mu\Omega$, an order of magnitude increase compared to HQ01e. The measured HQ02a dynamic harmonics can be reproduced with reasonable agreement (within 12%) by a simplified network model considering only the cross contact between strands. Based on this model, the effect of core width and position was studied. It is shown that the outer layer partially cancels the contribution to the ISCC multipole from the inner layer. For the same ISCC multipole reduction, a core placed in inner layer only may be more effective than a core placed in both layers of the magnet. Random errors due to local variations of R_c were analyzed. A mean R_c of 8 $\mu\Omega$ is necessary to limit the random error of ISCC multipoles at the nominal level below 0.1 units, assuming 20% of R_c variation among coil blocks.

Acknowledgment

The authors thank the engineering and technical staff of BNL, FNAL, and LBNL for their contributions to the magnet design, fabrication, and test. We also thank the FNAL engineering and technical staff for their support to the development of new magnetic measurement probes and associated equipment.

References

[1] M. N. Wilson, "NbTi superconductors with low ac loss: A review," *Cryogenics*, vol. 48, no. 7/8, pp. 381–395, Jul./Aug. 2008.
[2] L. Bottura, "Field dynamics in superconducting magnets for particle accelerators," in *CERN Accel. School, Meas. Alignment Accel. Detect. Magn.*, 1997, pp. 79–105.
[3] R. Bailey, F. Bordry, L. Bottura, P. Burla, P. Collier, K. Henrichsen, J. P. Koutchouk, R. Lauckner, R. Parker, J. Pett, P. Proudlock, H. Schmickler, R. Schmidt, L. Walckiers, and R. Wolf, "Dynamic effects and their control at the LHC," in *Proc. PAC*, 1997, pp. 66–68.
[4] A. den Ouden, S. Wessel, E. Krooshoop, and H. ten Kate, "Application of Nb_3Sn superconductors in high-field accelerator magnets," *IEEE Trans. Appl. Supercond.*, vol. 7, no. 2, pp. 733–738, Jun. 1997.
[5] R. Benjegerdes, P. Bish, S. Caspi, K. Chow, D. Dietderich, R. Hannaford, W. Harnden, H. Higley, A. Lietzke, A. McInturff, L. Morrison, M. Morrison, R. Scanlan, J. Smithwick, and C. Taylor, "Operational characteristics, parameters, history of a (13 T) Nb_3Sn dipole," in *Proc. Particle Accel. Conf.*, 1999, pp. 3233–3235.
[6] G. V. Velev, R. Bossert, S. Caspi, G. Chlachidze, J. DiMarco, P. Ferracin, V. V. Kashikhin, M. Lamm, G. L. Sabbi, P. Schlabach, M. Tartaglia, J. C. Tompkins, and A. V. Zlobin, "Field quality measurements and analysis of the LARP technology quadrupole models," *IEEE Trans. Appl. Supercond.*, vol. 18, no. 2, pp. 184–187, Jun. 2008.
[7] A. P. Verweij, "Electrodynamics of superconducting cables in accelerator magnets," Ph.D. dissertation, Univ. Twente, Enschede, The Netherlands, 1995.
[8] J. D. Adam, D. Leroy, L. R. Oberli, D. Richter, M. Wilson, R. Wolf, H. Higley, A. D. McInturff, R. M. Scanlan, A. Nijhuis, H. H. J. ten Kate, and S. Wessel, "Rutherford cables with anisotropic transverse resistance," *IEEE Trans. Appl. Supercond.*, vol. 7, no. 2, pp. 958–961, Jun. 1997.
[9] M. Sumption, E. Collings, R. Scanlan, A. Nijhuis, and H. ten Kate, "Core-suppressed AC loss and strand-moderated contact resistance in a Nb_3Sn Rutherford cable," *Cryogenics*, vol. 39, no. 1, pp. 1–12, Jan. 1999.
[10] N. Andreev, D. Chichili, C. Christensen, J. DiMarco, V. Kashikhin, P. Schlabach, C. Sylvester, I. Terechkine, J. C. Tompkins, G. Velev, and A. V. Zlobin, "Field quality of the Fermilab Nb_3Sn high field dipole model," in *Proc. Particle Accel. Conf.*, 2001, pp. 3418–3420.
[11] P. Ferracin, "LARP Nb_3Sn quadrupole magnets for the LHC luminosity upgrade," in *Proc. Adv. Cryog. Eng., Trans. Cryog. Eng. Conf.*, 2010, vol. 55, pp. 1291–1300.
[12] G. Sabbi, " Nb_3Sn IR quadrupoles for the high luminosity LHC," *IEEE Trans. Appl. Supercond.*, vol. 23, no. 3, p. 4000707, Jun. 2013.

[13] L. Bottura, G. de Rijk, L. Rossi, and E. Todesco, "Advanced accelerator magnets for upgrading the LHC," *IEEE Trans. Appl. Supercond.*, vol. 22, no. 3, p. 4002008, Jun. 2012.

[14] E. Todesco, H. Allain, G. Ambrosio, F. Borgnolutti, F. Cerutti, D. Dietderich, L. S. Esposito, H. Felice, P. Ferracin, G. Sabbi, P. Wanderer, and R. Van Weelderen, "Design studies for the low-beta quadrupoles for the LHC luminosity upgrade," *IEEE Trans. Appl. Supercond.*, vol. 23, no. 3, p. 4002405, Jun. 2013.

[15] E. Collings, M. Sumption, M. Susner, D. Dietderich, E. Krooshoop, and A. Nijhuis, "Interstrand contact resistance and magnetization of Rutherford cables with cores of different materials and widths," *IEEE Trans. Appl. Supercond.*, vol. 22, no. 3, p. 6000904, Jun. 2012.

[16] J. DiMarco, G. Ambrosio, M. Buehler, G. Chlachidze, D. Orris, C. Sylvester, M. Tartaglia, G. Velev, M. Yu, A. V. Zlobin, A. Ghosh, J. Schmalzle, P. Wanderer, F. Borgnolutti, D. Cheng, D. Dietderich, H. Felice, A. Godeke, R. Hafalia, J. Joseph, J. Lizarazo, M. Marchevsky, S. O. Prestemon, G. L. Sabbi, A. Salehi, X. Wang, P. Ferracin, and E. Todesco, "Field quality measurements of LARP Nb_3Sn magnet HQ02," *IEEE Trans. Appl. Supercond.*, to be published.

[17] H. Felice, G. Ambrosio, M. Anerella, R. Bossert, S. Caspi, D. Cheng, D. R. Dietderich, P. Ferracin, A. K. Ghosh, R. Hafalia, C. R. Hannaford, V. Kashikhin, J. Schmalze, S. Prestemon, G. L. Sabbi, P. Wanderer, and A. V. Zlobin, "Design of HQ—A high field large bore quadrupole magnet for LARP," *IEEE Trans. Appl. Supercond.*, vol. 19, no. 3, pp. 1235–1239, Jun. 2009.

[18] S. Caspi, G. Ambrosio, M. Anerella, E. Barzi, R. Bossert, D. Cheng, D. Dietderich, H. Felice, P. Ferracin, A. Ghosh, R. Hafalia, R. Hannaford, V. V. Kashikhin, D. Pasholk, G. L. Sabbi, J. Schmalzle, P. Wanderer, and A. Zlobin, "Design of a 120 mm bore 15 T quadrupole for the LHC upgrade phase II," *IEEE Trans. Appl. Supercond.*, vol. 20, no. 3, pp. 144–147, Jun. 2010.

[19] H. Felice, G. Ambrosio, M. Anerella, D. Bocian, R. Bossert, S. Caspi, B. Collins, D. Cheng, G. Chlachidze, D. R. Dietderich, P. Ferracin, A. Godeke, A. Ghosh, A. R. Hafalia, J. M. Joseph, J. Krishnan, M. Marchevsky, G. Sabbi, J. Schmalzle, P. Wanderer, X. R. Wang, and A. Zlobin, "Impact of coil compaction on LARP HQ magnet," *IEEE Trans. Appl. Supercond.*, vol. 22, no. 3, p. 4001904, 2012.

[20] D. Dietderich and A. Godeke, "Nb_3Sn research and development in the USA—Wires and cables," *Cryogenics*, vol. 48, no. 7/8, pp. 331–340, Jul./Aug. 2008.

[21] A. K. Jain, "Basic theory of magnets," in *CERN Accel. School, Meas. Alignment Accel. Detect. Magn.*, 1998, pp. 1–26, CERN-98-05.

[22] J. DiMarco, G. Chlachidze, A. Makulski, D. Orris, M. Tartaglia, J. Tompkins, G. V. Velev, and X. Wang, "Application of PCB and FDM technologies to magnetic measurement probe system development," *IEEE Trans. Appl. Supercond.*, vol. 23, no. 3, p. 9000505, Jun. 2013.

[23] X. Wang, S. Caspi, D. W. Cheng, D. R. Dietderich, H. Felice, P. Ferracin, A. Godeke, R. Hafalia, M. Joseph, J. Lizarazo, M. Marchevsky, G. L. Sabbi, A. Ghosh, J. Schmalzle, P. Wanderer, G. Ambrosio, R. Bossert, G. Chlachidze, J. DiMarco, V. Zlobin, A. Milanese, and E. Todesco, "Summary of HQ01e magnetic measurements," Lawrence Berkeley Nat. Lab., Berkeley, CA, USA, Tech. Rep. LBNL-5290E, 2012.

[24] S. Caspi, G. Ambrosio, M. Anerella, E. Barzi, B. Bingham, R. Bossert, D. W. Cheng, G. Chlachidze, D. R. Dietderich, H. Felice, P. Ferracin, A. Ghosh, A. R. Hafalia, C. R. Hannaford, J. Joseph, V. V. Kashikhin, G. L. Sabbi, J. Schmalzle, P. Wanderer, W. Xiaorong, and A. V. Zlobin, "Test results of 15 T quadrupole magnet HQ01 with a 120 mm bore for the LHC luminosity upgrade," *IEEE Trans. Appl. Supercond.*, vol. 21, no. 3, pp. 1854–1857, Jun. 2011.

[25] M. Marchevsky, G. Ambrosio, B. Bingham, R. Bossert, S. Caspi, D. W. Cheng, G. Chlachidze, D. Dietderich, J. Dimarco, H. Felice, P. Ferracin, A. Ghosh, A. R. Hafalia, J. Joseph, J. Lizarazo, G. L. Sabbi, J. Schmalzle, P. Wanderer, X. Wang, and A. V. Zlobin, "Quench performance of HQ01, a 120 mm bore LARP quadrupole for the LHC upgrade," *IEEE Trans. Appl. Supercond.*, vol. 22, no. 3, p. 4702005, Jun. 2012.

[26] H. Bajas, G. Ambrosio, M. Anerella, M. Bajko, R. Bossert, S. Caspi, A. Chiuchiolo, G. Chlachidze, D. Dietderich, O. Dunkel, H. Felice, P. Ferracin, J. Feuvrier, L. Fiscarelli, A. Ghosh, C. Giloux, A. Godeke, A. R. Hafalia, M. Marchevsky, S. Russenschuck, G. L. Sabbi, T. Salmi, J. Schmalzle, E. Todesco, P. Wanderer, X. Wang, and M. Yu, "Cold test results of the LARP HQ Nb_3Sn quadrupole magnet at 1.9 K," *IEEE Trans. Appl. Supercond.*, vol. 23, no. 3, p. 4002606, Jun. 2013.

[27] S. Russenschuck, *Field Computation for Accelerator Magnets: Analytical and Numerical Methods for Electromagnetic Design and Optimization*. Hoboken, NJ, USA: Wiley, 2010.

[28] K.-H. Mess, P. Schmüser, and S. Wolff, *Superconducting Accelerator Magnets*. Singapore: World Scientific, 1996, ch. 5, pp. 65–69.

[29] S. Redaelli, "Analysis of the magnetic field perturbations in dipoles and quadrupoles of the large hadron collider (LHC)," Ph.D. dissertation, The University of Milan, Milan, Italy, 2000.

[30] E. Collings, M. Sumption, M. Susner, D. Dietderich, and A. Nijhuis, "Coupling loss, interstrand contact resistance, magnetization of Nb_3Sn Rutherford cables with cores of MgO tape and S-glass ribbon," *IEEE Trans. Appl. Supercond.*, vol. 21, no. 3, pp. 2367–2371, Jun. 2011.

[31] T. Ogitsu, V. Kovachev, and A. Devred, "Influence of inter-strand coupling current on field quality of superconducting accelerator magnets," *Part. Accel.*, vol. 57, pp. 215–235, 1997.

[32] R. Wolf, D. Leroy, D. Richter, A. Verweij, and L. Walckiers, "Determination of interstrand contact resistance from loss and field measurements in LHC dipole prototypes and correlation with measurements on cable samples," *IEEE Trans. Appl. Supercond.*, vol. 7, no. 2, pp. 797–800, Jun. 1997.

[33] G. Chlachidze, G. Ambrosio, M. Anerella, F. Borgnolutti, R. Bossert, S. Caspi, D. W. Cheng, D. Dietderich, H. Felice, P. Ferracin, A. Ghosh, A. Godeke, A. R. Hafalia, M. Marchevsky, D. Orris, P. K. Roy, G. L. Sabbi, T. Salmi, J. Schmalzle, C. Sylvester, M. Tartaglia, J. Tompkins, P. Wanderer, X. R. Wang, and A. V. Zlobin, "Performance of HQ02, an optimized version of the 120 mm Nb_3Sn LARP quadrupole," *IEEE Trans. Appl. Supercond.*, to be published.

[34] M. Di Castro, L. Bottura, D. Richter, S. Sanfilippo, and R. Wolf, "Coupling current and AC loss in LHC superconducting quadrupoles," *IEEE Trans. Appl. Supercond.*, vol. 18, no. 2, pp. 108–111, Jun. 2008.

[35] G. L. Sabbi, private communication, 2013.

[36] A. den Ouden, W. Wessel, H. Krooshoop, H. van Weeren, H. ten Kate, G. Kirby, R. Ostojic, T. Taylor, and N. Siegel, "Conductor related design considerations for a 1 meter 10 T Nb_3Sn dipole magnet," *IEEE Trans. Appl. Supercond.*, vol. 13, no. 2, pp. 1288–1291, Jun. 2003.

[37] P. Ferracin, W. Scandale, E. Todesco, and R. Wolf, "Modeling of random geometric errors in superconducting magnets with applications to the CERN large hadron collider," *Phys. Rev. ST Accel. Beams*, vol. 3, pp. 122403-1–122403-9, 2000.